A Simple Chaotic Flow with Hyperbolic Sinusoidal Function and Its Application to Voice Encryption

Saleh Mobayen [1] [iD]**, Christos Volos** [2,*] [iD]**, Ünal Çavuşoğlu** [3] **and Sezgin S. Kaçar** [4] [iD]

[1] Future Technology Research Center, National Yunlin University of Science and Technology, 123 University Road, Section 3, Douliou, Yunlin 64002, Taiwan; mobayens@yuntech.edu.tw

[2] Laboratory of Nonlinear Systems, Circuits & Complexity (LaNSCom), Department of Physics, Aristotle University of Thessaloniki, GR-54124 Thessaloniki, Greece

[3] Department of Software Engineering, Sakarya University, Sakarya 54050, Turkey; unalc@sakarya.edu.tr

[4] Department of Electrical and Electronics Engineering, Sakarya University of Applied Sciences, Sakarya 54050, Turkey; skacar@subu.edu.tr

* Correspondence: volos@physics.auth.gr

check for updates

Abstract: In this article, a new chaotic system with hyperbolic sinusoidal function is introduced. This chaotic system provides a new category of chaotic flows which gives better perception of chaotic attractors. In the proposed chaotic flow with hyperbolic sinusoidal function, according to the changes of parameters of the system, the self-excited attractor and two forms of hidden attractors are occurred. Dynamic behavior of the offered chaotic flow is studied through eigenvalues, bifurcation diagrams, phase portraits, and spectrum of Lyapunov exponents. Moreover, the existence of double-scroll attractors in real word is considered via the Orcard-PSpice software through an electronic execution of the new chaotic flow and illustrative results between the numerical simulation and Orcard-PSpice outcomes are obtained. Lastly, random number generator (RNG) design is completed with the new chaos. Using the new RNG design, a novel voice encryption algorithm is suggested and voice encryption use and encryption analysis are performed.

Keywords: chaotic flow; hyperbolic sinusoidal function; hidden attractor; voice encryption; symmetry

1. Introduction

Chaotic flows are mathematical models originated from the rules of defining chaotic behaviors [1,2]. In the former decades, the chaos theory has been employed in numerous fields such as digital signature [3], secure cryptography [4], pseudorandom number generation [5], secure communication [6], weak signal detection [7], DC-DC boost converter [8], image encryption [9], neurophysiology [10], secure data transmission [11], etc. For the control and synchronization purposes of chaotic systems, several techniques like active control [12], fuzzy control [13], linear matrix inequality (LMI) [14], sampled-data control [15], impulsive adaptive control [16], intermittent control [17] and sliding mode control (SMC) [18] have been introduced.

Recently, Wei (2011) announced a chaotic system with no equilibrium point [19]. Jafari et al. (2013) discovered a set of 17 elementary quadratic chaos systems with no equilibrium points [20]. A chaos system possessing a stable equilibrium point was recently found in [21,22]. It is observed that Shilnikov method [23,24] is not applicable to check chaos behavior in special dynamical systems with no equilibrium point or with stable equilibrium points. Such dynamical systems can be viewed as systems with hidden chaotic attractors in scientific computing [24–26]. Chaotic systems with hidden attractors can result in unexpected disastrous behavior in mechanical systems and electronic circuits.

It is stimulating that chaotic flows containing infinite number of equilibrium points have achieved much consideration in the past decade. Especially, structures with uncountable equilibrium points

are categorized as systems with hidden attractors [27,28]. Hidden attractors do not have basins of attraction related to the unstable equilibria. As stated by the recent investigations, hidden attractors are fundamental in engineering usages, for instance, radio-physical oscillator [29], multilevel DC/DC converter [30], electromechanical systems [31] or relay system with hysteresis [32].

In recent years, some new chaotic flows have been planned via cascade chaos, dimension expansion, and physics modelling [1,33]. An extensive body of scientists has been devoted on counteracting degradation and performance improvement of existing chaotic flows. As chaos is broadly employed in nonlinear control, synchronization, and other usages, the design problem of the chaotic flows with complex chaotic behaviors is more attractive [34].

In addition, a widespread application of chaotic systems is that of encryption schemes, voice, text or image. In these schemes, RNGs are the most basic constructs. The fact that the numbers used in encryption have a high randomness and a big impact on the quality of the encryption. In the last few years, some encryption schemes, especially for sound messages, based mainly on discrete chaotic maps, have been presented. In 2016, Sadkhan et al. presented a new speech scrambling system using a hybrid use of different chaotic maps [35]. In 2018, Mobayen et al. proposed the implementation of a sound encryption method based on a novel chaotic system with boomerang-shaped equilibrium [36]. On the same year, Raheema et al. presented an efficient Simulink model, speech scrambling based chaotic maps for encryption of data such as voice, video and text, because it possesses high sensitive to initial values and model external parameters [37].

The objective of this article is to investigate a novel chaotic flow with hyperbolic sinusoidal function. The proposed chaotic flow provides a new category of chaotic systems which helps in more perception of chaotic attractors. In this chaotic flow, because of the variations of the parameters, the self-excited attractor and two forms of hidden attractors (no equilibrium point and line of equilibria) are created. Next, the proposed chaotic system with hidden attractors has been used in the design of an RNG algorithm. Finally, this RNG algorithm is used in a sound encryption scheme.

The rest of this work is organized as follows. In the following section, mathematical form of new chaotic structure is given and different scenarios are proposed. Moreover, some discussions for chaotic flow covering dynamic features such as spectrum of the Lyapunov exponents, bifurcation diagrams, and Poincaré map are proposed. In Section 3, the circuit design of presented chaotic flow is provided and PSpice representation of the chaotic attractors is presented. In Section 4, the engineering application containing RNG algorithm design and voice encryption algorithm is described. As a final point, conclusions are provided in Section 5.

2. Chaotic Flow with a Hyperbolic Sinusoidal Function

In the search for chaos flows with hyperbolic sinusoidal function, we study the form of a three-dimensional chaotic structure as:

$$\begin{aligned}
\dot{x} &= a_1 x + a_2 y + a_3 z + a_4 xy + a_5 xz + a_6 yz + b, \\
\dot{y} &= a_7 xy + a_8 xz + a_9 yz + a_{10} sinh(y) + c, \\
\dot{z} &= a_{11} x + a_{12} y + a_{13} z + a_{14} xy + a_{15} xz + a_{16} yz
\end{aligned} \tag{1}$$

where x, y and z denote the system states; $a_1, \ldots, a_{16}$ indicate the coefficients of the terms; b and c are two scalars which define the chaos behavior.

A computer examination is executed investigating millions of combinations of different forms, various initial states and different constant values, looking for dissipative cases for which the largest Lyapunov exponent is bigger than 0.001. The system is in chaos state if the largest Lyapunov exponent is bigger than zero, and the system is in steady period state if the largest Lyapunov exponent is smaller

than zero [38,39]. Therefore, in the present work, a three-dimensional chaotic flow is reported which is specified by:

$$\begin{aligned} \dot{x} &= x - ayz + b, \\ \dot{y} &= xz - sinh(y) + c, \\ \dot{z} &= x \end{aligned} \tag{2}$$

where the parameter a_6 in (1) has been denoted as parameter a in system (2).

Next, three different scenarios depending on the values of system's (2) parameters b, c are discussed in details.

2.1. Scenario A: Line of Equilibria

If $b = c = 0$, the chaotic flow (2) will have a line of equilibria, i.e., $E_A = [0, 0, z^*]^T$, where z^* is the equilibrium point value in z axis and T means the transpose of the vector. To analyze the state trajectories in the vicinity of the equilibrium point, the Jacobian matrix is obtained from (2) as:

$$J = \begin{bmatrix} 1 & -az & -ay \\ z & -cosh(y) & x \\ 1 & 0 & 0 \end{bmatrix}. \tag{3}$$

For equilibrium point $E_A = [0, 0, z^*]^T$, the Jacobian matrix is defined as

$$J = \begin{bmatrix} 1 & -az^* & 0 \\ z^* & -1 & 0 \\ 1 & 0 & 0 \end{bmatrix}. \tag{4}$$

Therefore, the eigenvalues of the linearized system are achieved as

$$|\lambda I - J| = \begin{vmatrix} \lambda - 1 & az^* & 0 \\ -z^* & \lambda + 1 & 0 \\ -1 & 0 & \lambda \end{vmatrix} = \lambda\left(\lambda^2 + az^{*2} - 1\right) = 0 \Rightarrow \lambda_1 = 0, \lambda_{2,3} = \pm \sqrt{1 - az^{*2}}. \tag{5}$$

The equilibrium is a saddle node for $-\frac{1}{\sqrt{a}} < z^* < \frac{1}{\sqrt{a}}$. The equilibrium point is an unstable node for $z^* = \pm\frac{1}{\sqrt{a}}$. For the values $z^* > \frac{1}{\sqrt{a}}$ and $z^* < -\frac{1}{\sqrt{a}}$, since one eigenvalue is zero and two eigenvalues are imaginary, the stability of the equilibrium point cannot be determined by this method; the equilibrium point may be stable, unstable or marginally stable.

If one design parameter is varied and the norm of the state variables vector is plotted for finding the fixed points of the system versus the changing parameter, finally the bifurcation diagram is obtained [40]. In the bifurcation diagrams, the fixed points maybe disappear, appear, or change their stability nature when the design parameter is changed. Those variations may occur even for infinitesimal changes in the parameter. Bifurcation diagram is used for the stability analysis of a dynamical system [41,42]. Moreover, the Lyapunov exponents spectrum makes it possible to qualitatively quantify a local property with respect to the attractor's stability. The positive/negative values of the Lyapunov exponents can be observed as a measure of the averaged exponential divergence/convergence of neighborhood trajectories [43,44]. The bifurcation diagram for y, when the states cut the plane $z = 0$ with $dz/dt < 0$, as well as the spectrum of system's Lyapunov exponents (LE_i, $i = 1, 2, 3$), by varying the value of a to explore the dynamical form of system (2), while keeping the initial states as $[x_0, y_0, z_0] = [2, 0.2, 1]$, are depicted in Figure 1. Therefore, the suggested structure (2) is integrated via the classical Runge-Kutta integration algorithm [45], numerically. For all of the parameters, the simulation calculations are executed via the parameters and variables in extended precision mode. In addition, the spectrum of the Lyapunov exponents are found via the Wolf's algorithm [46].

(a)

(b)
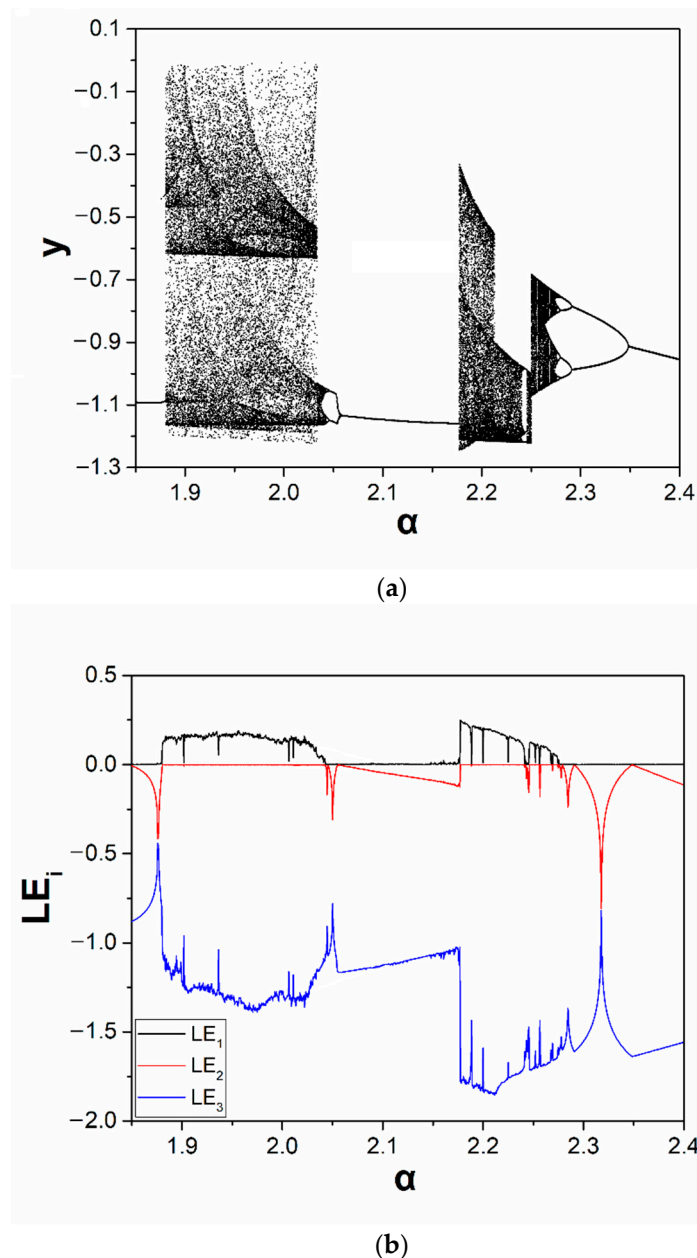
Figure 1. (**a**) Bifurcation diagram, (**b**) Lyapunov exponents spectrum of dynamics (2), when changing *a* from 1.85 to 2.4, and *b* = *c* = 0.

The dynamics (2) shows a chaotic attractor, for *a* = 2 (Figure 2), and a limit cycle of Period-1, for *a* = 2.35 (Figure 3). The spectrum of Lyanpunov exponents (Figure 1b) approves the dynamic behavior of the system as it has been revealed via bifurcation diagram.

2.2. Scenario B: No Equilibrium Point

If $b \neq 0$, $c = 0$ and by keeping $a = 2$, for obtaining the equilibrium point, we solve $\dot{x} = 0$, $\dot{y} = 0$ and $\dot{z} = 0$, that is

$$
\begin{aligned}
x - 2yz + b &= 0, \\
xz - sinh(y) &= 0, \\
x &= 0.
\end{aligned}
\tag{6}
$$

Consequently, the chaotic flow has no equilibrium point in this case. Therefore, it belongs to the category of chaotic systems containing hidden attractors.

Taking the bifurcation diagram of *y* (Figure 4a), along with the Lyapunov exponents spectrum (Figure 4b) by changing *b* for $0 < b < 0.005$, in order to explore the dynamics (2), for initial conditions $[x_0, y_0, z_0] = [2, 0.2, 1]$, interesting dynamical behavior has been investigated. As it is obtained from bifurcation diagram (Figure 4a), the system passes from a chaotic region, for $b \in [0, 0.075)$, to a periodic one as the parameter *b* increases.
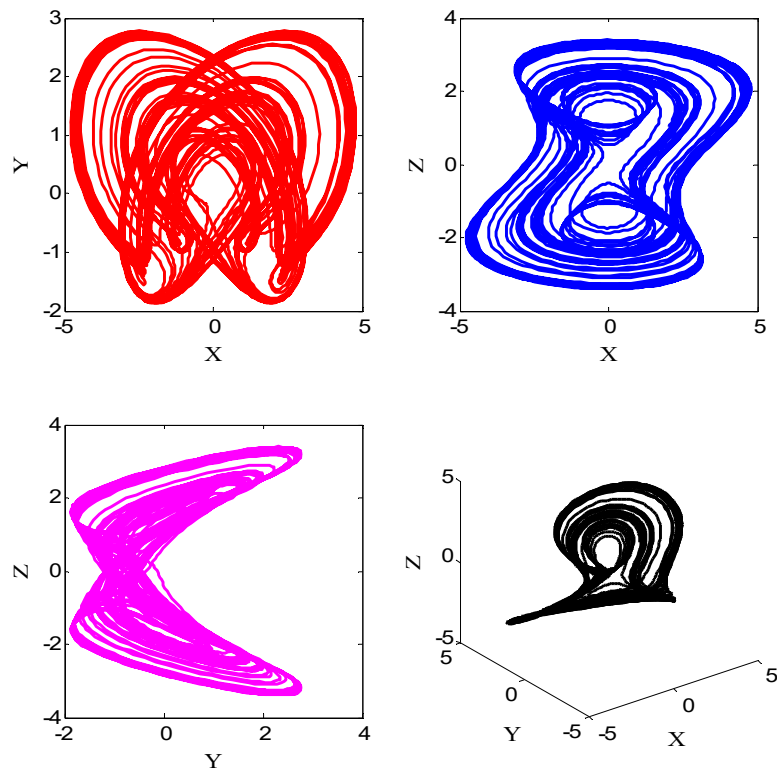

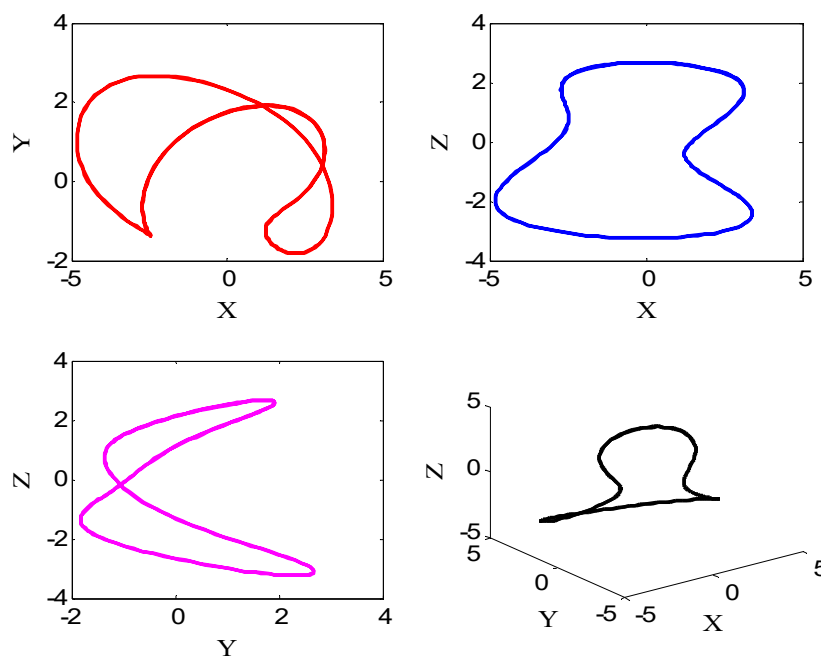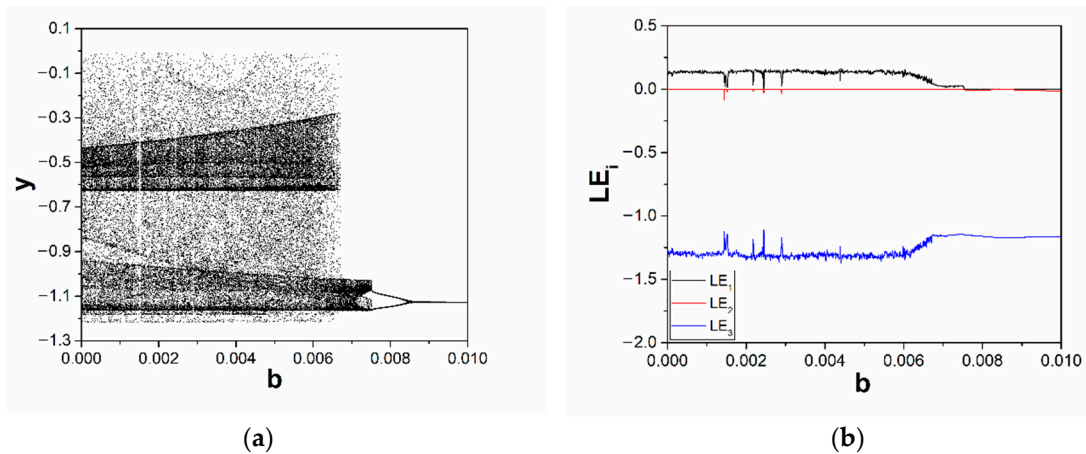**Figure 2.** Strange chaos attractor for *a* = 2 and *b* = *c* = 0 in Scenario A.


**Figure 3.** Limit cycle of period-1 for *b* = *c* = 0 and *a* = 2.35 in Scenario A.

Figure 4. (**a**) Bifurcation diagram, (**b**) spectrum of Lyapunov exponents of (2), when changing b from 0 to 0.01, for $a = 2$, $c = 0$.

The strange attractors of the system (2) are displayed for $a = 2$, $b = 0.005$ and $c = 0$ in Figure 5. In this case, the Lyapunov exponents are $LE_1 = 0.14107$, $LE_2 = 0$, $LE_3 = -1.33835$, which confirmed the chaotic behavior of the system (2). The Kaplan-York dimension of the chaotic flow is $D_{KY} = 2.1054$. Besides, the Poincaré map in x-y plane presents the folding properties of chaos when $z = 0$ with $dz/dt < 0$ (Figure 6).
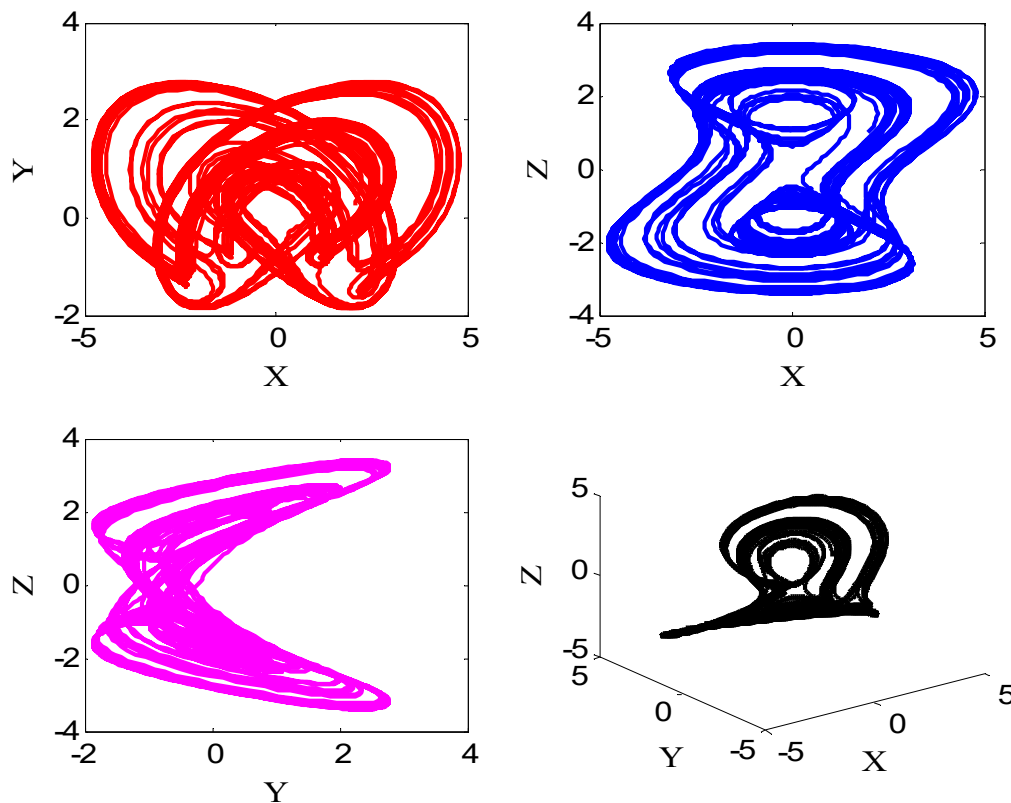
Figure 5. Strange chaotic attractors for $a = 2$, $b = 0.005$ and $c = 0$.
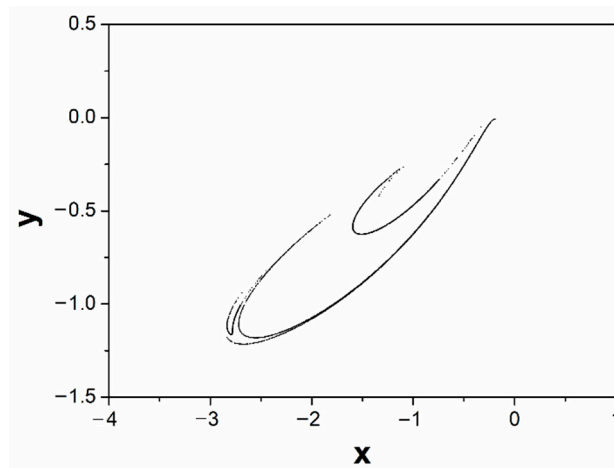
Figure 6. Poincaré map of chaotic system (2) in the x–y plane, for $a = 2$, $b = 0.005$ and $c = 0$.

2.3. Scenario C: Self-Excited Attractor

If $b = 0$, $c \neq 0$ and $a = 2$ this chaotic flow has only one equilibrium $E_C = \left[0, sinh^{-1}(b), 0\right]^T$. For the equilibrium point E_C, the Jacobian matrix is found as:

$$J = \begin{bmatrix} 1 & 0 & -2sinh^{-1}(b) \\ 0 & -cosh(sinh^{-1}(b)) & 0 \\ 1 & 0 & 0 \end{bmatrix}. \tag{7}$$

Then, the eigenvalues of the linearized chaotic flow are obtained as:

$$\begin{aligned} |\lambda I - J| &= \begin{vmatrix} \lambda - 1 & 0 & 2sinh^{-1}(c) \\ 0 & \lambda + cosh(sinh^{-1}(c)) & 0 \\ -1 & 0 & \lambda \end{vmatrix} \\ &= \left(\lambda + cosh(sinh^{-1}(c))\right)\left(\lambda^2 - \lambda + 2sinh^{-1}(c)\right) = 0 \\ &\Rightarrow \lambda_1 = -cons(sinh^{-1}(c)) = -\sqrt{1 + c^2}, \lambda_{2,3} = \frac{1 \pm \sqrt{1 - 8sinh^{-1}(c)}}{2}. \end{aligned} \tag{8}$$

For $c > 0.1253$, the eigenvalues of the chaotic flow are found as $\lambda = -\sqrt{1 + c^2}, \frac{1 \pm i\omega}{2}$, and the equilibrium point is a saddle focus. For $c < 0.1253$, the eigenvalues of the chaotic flow are obtained as $\lambda = -\sqrt{1 + c^2}, \frac{1 \pm \sqrt{\Delta}}{2}$, and the equilibrium point is a saddle node.

Figure 7 depicts the bifurcation diagram of variable y as well as the spectrum of Lyapunov exponents by varying c, for $0 < c < 0.05$, to explore the dynamics (2), for initial states $[x_0, y_0, z_0] = [2, 0.2, 1]$. It is shown from bifurcation diagram (Figure 7a) that the system passes from a chaotic region for $c \in [0, 0.0285)$ to a periodic one as the parameter c increases. The respective spectrum of Lyapunov exponents to parameter c displays the aforementioned system's (2) dynamical behavior for $a = 2$ and $b = 0$.

The strange attractors of (2) for $a = 2$, $b = 0$, and $c = 0.02$ are demonstrated in Figure 8. For these parameter's values, the Lyapunov exponents are $LE_1 = 0.09822$, $LE_2 = 0$, $LE_3 = -1.27669$, which confirmed the chaotic behavior of system (2). The Kaplan-York dimension is $D_{KY} = 2.07699$. Furthermore, the Poincaré maps in x–y plane, when $z = 0$ with $dz/dt < 0$ (Figure 9) presents the folding features of chaos.

(**a**)

(**b**)
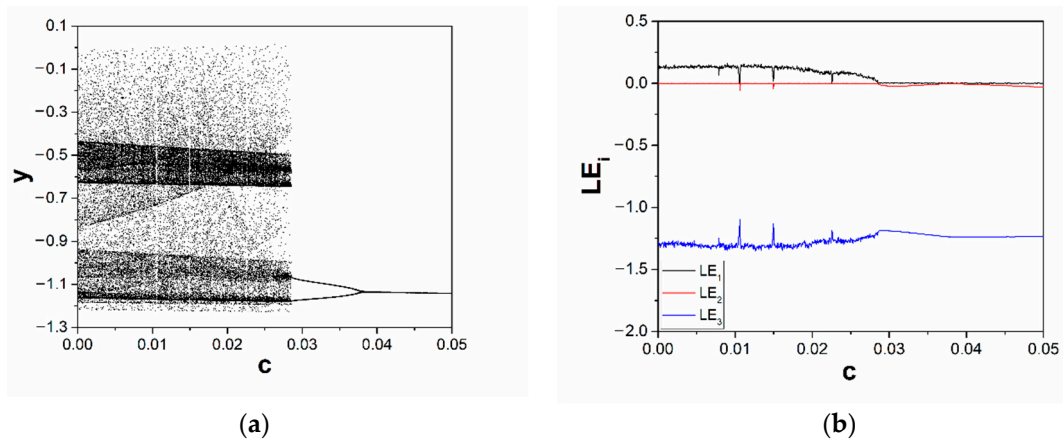
Figure 7. (**a**) Bifurcation diagram, (**b**) Lyapunov exponents spectrum of (2) when changing *c* from 0 to 0.05, for $a = 2$, $b = 0$.
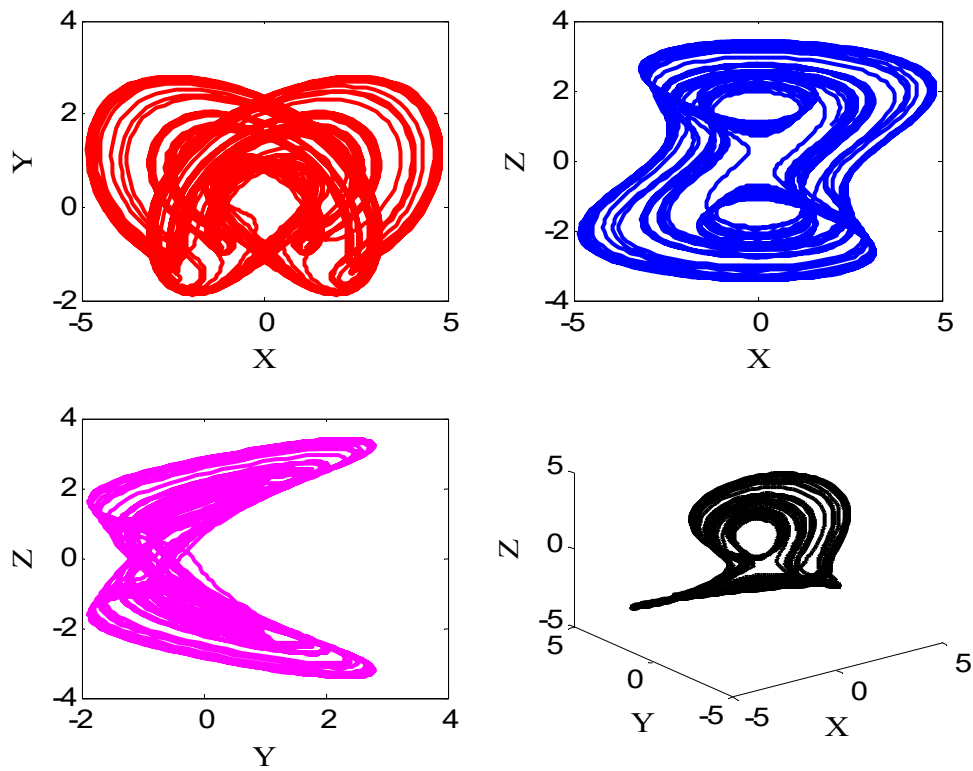
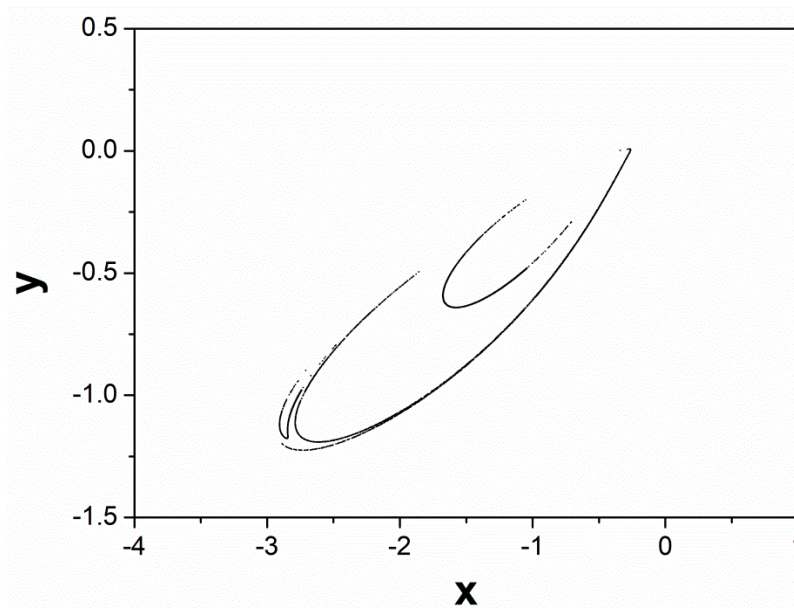**Figure 8.** Strange attractors for $a = 2$, $b = 0$ and $c = 0.02$.

Figure 9. Poincaré map of system (2) in the *x-y* plane, for *a* = 2, *b* = 0 and *c* = 0.02.

3. Circuit Design of the Proposed Chaotic Flow

In recent years, the physical realizations of theoretical chaos forms have been investigated extensively for approving the feasibility and employing them in practical usages [47–50]. Therefore, in this section, a circuit realization with the hyperbolic sinusoidal nonlinearity is presented. For the reason of easiness, the general design methodology is applied according to the operational amplifiers [51,52]. The circuit is designed by using the common electronic components as displayed in Figure 10. There are an inverting amplifier (U4), three integrators (U1–U3), and two analog multipliers (U7, U8) of type AD633. The circuit for simulating the hyperbolic sinusoidal nonlinearity, in the dotted frame, includes three resistors (R_{S1}–R_{S3}), two operational amplifiers (U5, U6) and two diodes (D_1, D_2).

Based on Figure 8, via the Kirchhoff's laws, the circuital equation of the circuit is found as

$$\dot{X} = \frac{1}{RC}\left[X - \frac{R}{R_1 1V}YZ + V_b\right],$$
$$\dot{Y} = \frac{1}{RC}\left[\frac{XZ}{1V} - \frac{2I_S R_{S3} R}{R_4}sinh\left(\frac{R_{S2}}{nV_T R_{S1}}\right) + V_c\right], \tag{9}$$
$$\dot{Z} = \frac{1}{RC}X$$

where I_S, n and V_T are diode's reverse bias saturation current, the diode's ideality factor, and the thermal voltage, correspondingly. Normalizing the Equation (9) with $\tau = t/RC$, the dimensionless structure can be designated by

$$\dot{X} = X - \frac{R}{R_1 1V}YZ + V_b,$$
$$\dot{Y} = \frac{XZ}{1V} - \frac{2I_S R_{S3} R}{R_4}sinh\left(\frac{R_{S2}}{nV_T R_{S1}}\right) + V_c, \tag{10}$$
$$\dot{Z} = X$$

The variables (*X*, *Y*, *Z*) are equivalent to output voltages of integrators (U1–U3), when the power supply is ±15 V_{DC}. The system (10) corresponds to the suggested system with the hyperbolic sinusoidal nonlinear function (2). The electronic components are selected for *a* = 2, and *b* = *c* = 0; then we have *R* = R_4 = 30 kΩ, R_1 = 15 kΩ, R_2 = 10 kΩ, R_3 = 90 kΩ, R_{S1} = 100 kΩ, R_{S2} = 50.66 kΩ, R_{S3} = 18.65 MΩ and *C* = 10 nF. The planned circuit of Figure 10 has been executed in Multisim, and some PSpice results are presented in Figure 11. One can obviously confirm the consistency of the simulations (Figure 11) and numerical outcomes (Figure 2).
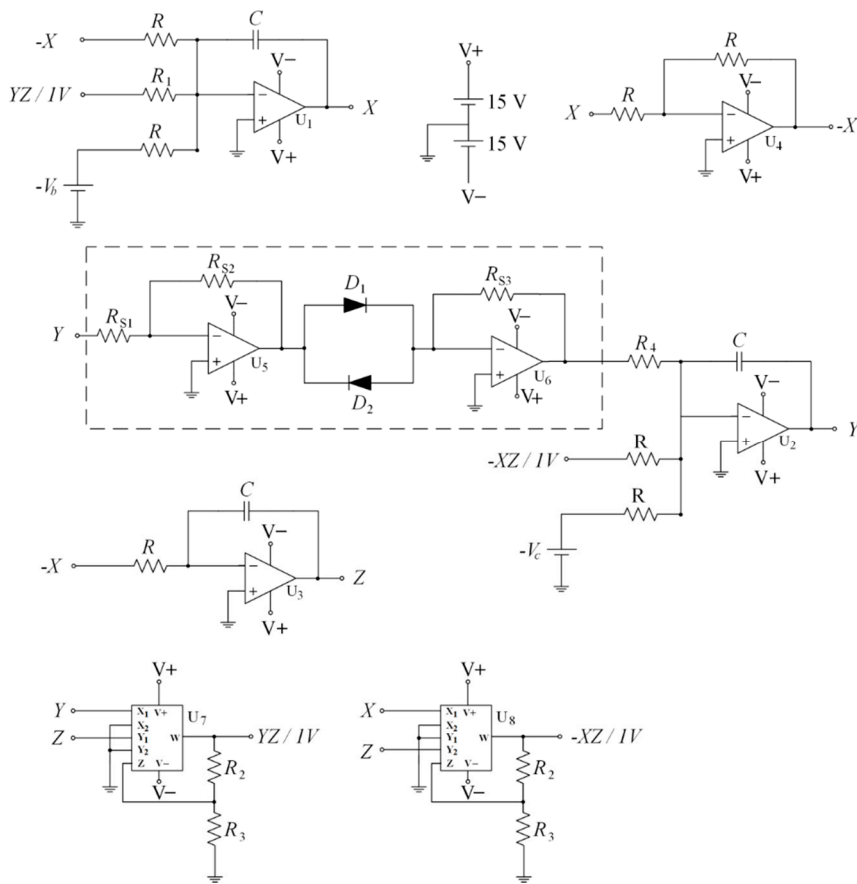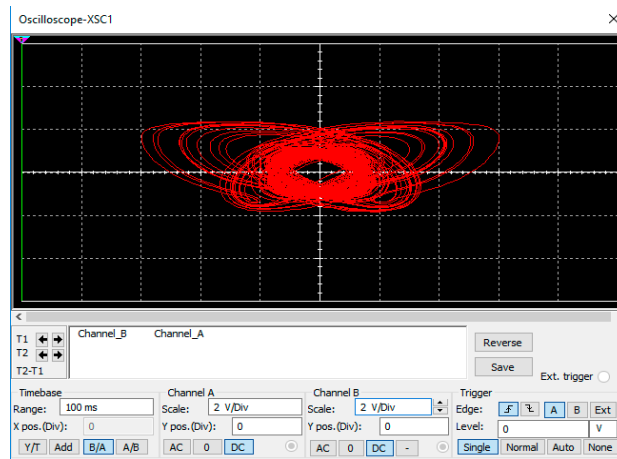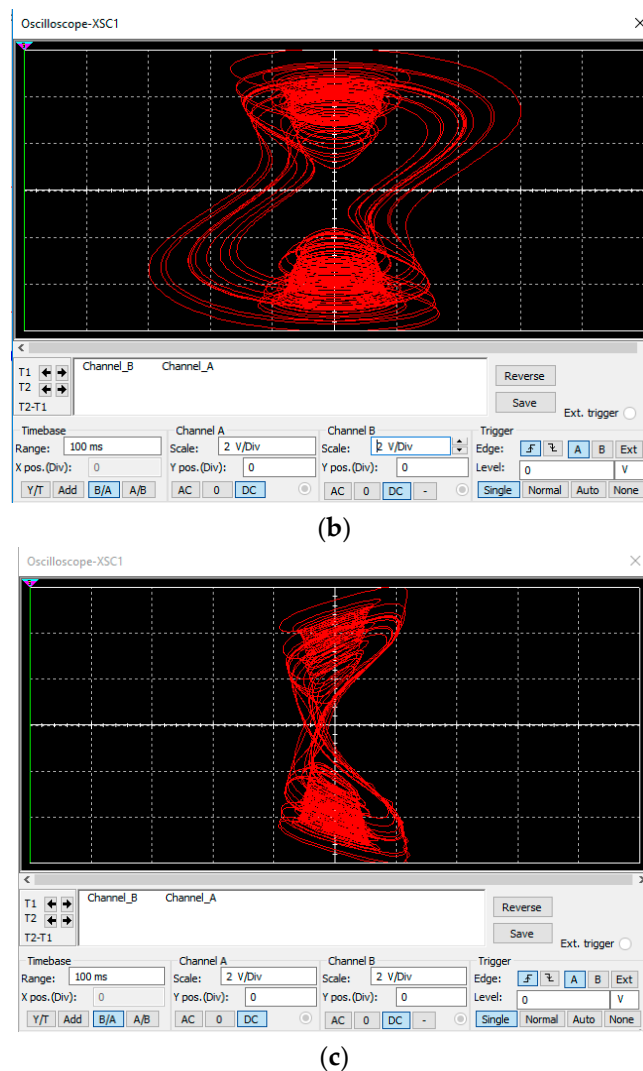
Figure 10. Schematic of circuit simulation for the system with hyperbolic sinusoidal nonlinear function (2).

(**a**)

Figure 11. *Cont.*

(b)

(c)

Figure 11. PSpice chaotic attractors of system with hyperbolic sinusoidal nonlinearity in (**a**) *X*–*Y* plane, (**b**) *X*–*Z* plane, and (**c**) *Y*–*Z* plane (*x*: 2 V/Div, *y*: 2 V/Div).

4. Voice Encryption Algorithm Design and Its Analysis

Chaos-based cryptography is one of the topics that has been intensively studied in recent years because of the randomness and rich dynamics of chaotic systems [53–58]. These works usually focus on image encryption. A new RNG algorithm design is performed by using the developed chaotic form and National Institute of Standards and Technology (NIST) 800-22 [59] randomness tests are employed to study the randomness of the obtained random numbers. It is noted that the NIST statistical test suit is used for the evaluation of the advanced encryption standard candidate algorithms. At first, a voice encryption algorithm is proposed using the obtained random number. Then, the voice encryption is executed by using the proposed algorithm and frequency spectrum analysis of the encryption procedure is executed.

4.1. RNG Algorithm Design and NIST 800-22 Test Results

In this subsection, an RNG algorithm design is developed via the newly introduced chaos in order to obtain the random numbers to be employed in the algorithm. The design process of the RNG algorithm is carried out as exposed in Algorithm 1 (see Appendix A). In the design process of the RNG algorithm, firstly the initial states and parameters of the chaotic system are defined. Then, the sampling interval of the system is determined and the chaotic system is considered by using

fourth-order Runge-Kutta (RK-4) integration algorithm using this sampling value. As an outcome of the system analysis, float values are found for each cycle from each phase. On the float values obtained from each phase, the step values of the decimal parts after the comma are subjected to the mode 2 operation. As a result, 15 bits are generated from each phase in the each cycle. Further, these obtained values are added to the number sequences for each phase (rngx, rngy, rngz). This process continues for each number sequence until the 1 M. bit is generated for the NIST 800-22 randomness examinations. Because at least 1 M. bit is needed for NIST 800-22 tests. After 1 M bits are generated from each phase, the phases are subjected to Exclusive Or (XOR) processing in binary form and new random number sequences are generated as named rngxy, rngxz, rngyz, rngxyz in the Algorithm 1. The generated values from the x and y phases are subjected to XOR processing to obtain a rngxy random number sequence. Similarly, generated from the phases y and z for rngyz, the *x* and *z* phases for rngyz and the x, y, z phases for rngxyz are subjected to XOR processing. Finally, NIST 800-22 tests are employed to all obtained random bit sequences. When random bit sequences are tested singularly, they cannot pass some tests. For this reason, random bit sequences generated are subjected to 2 or 3 XOR operations.

For the safe use of random numbers, they must have an appropriate randomness. The NIST 800-22 tests are a set of internationally accepted and frequently used tests in the literature that define the numbers' randomness via a variety of different tests. The NIST 800-22 test outcomes for the random number sequences originated from the developed RNG algorithm are displayed in Table 1. According to the test outcomes, it is seen that all the random numbers created passed all the examinations.

Table 1. NIST 800-22 NIST Test Results.

NIST Statistical Tests	*p*-Value ($x \oplus y$)	*p*-Value ($x \oplus z$)	*p*-Value ($y \oplus z$)	*p*-Value ($x \oplus y \oplus z$)	Results
Frequency (Monobit) Test	0.32708	0.70840	0.07409	0.83679	Passed
Block-Frequency Test	0.05028	0.44384	0.87530	0.24483	Passed
Cumulative-Sums Test	0.49997	0.79399	0.12548	0.88754	Passed
Runs Test	0.28235	0.05285	0.01530	0.34010	Passed
Longest-Run Test	0.91108	0.88963	0.46730	0.057827	Passed
Binary Matrix Rank Test	0.17994	0.15263	0.55596	0.39136	Passed
Discrete Fourier Transform Test	0.17441	0.92688	0.52063	0.20211	Passed
Overlapping Templates Test	0.63213	0.12006	0.96148	0.29966	Passed
Maurer's Universal Statistical Test	0.59708	0.81350	0.40059	0.48723	Passed
Approximate Entropy Test	0.95048	0.38285	0.27585	0.52635	Passed
Random-Excursions Test (x = −4)	0.82604	0.57997	0.40488	0.34822	Passed
Random-Excursions Variant Test (x = −4)	0.74935	0.63538	0.19136	0.46211	Passed
Serial Test-1	0.53650	0.89087	0.74965	0.92028	Passed
Serial Test-2	0.13577	0.48589	0.27236	0.75602	Passed
Linear-Complexity Test	0.72956	0.94527	0.31945	0.78612	Passed

4.2. Voice Encryption Algorithm Design and Its Application

A new voice encryption algorithm is developed via RNG algorithm introduced in the previous section, voice encryption usage and its analysis are performed. The block diagram of the encryption process is presented in Figure 12. In the encryption algorithm, after entering initial states and parameters of chaotic system, these values are transmitted to the receiving side as a key for generation of the random number sequences to be employed in the decryption process. In order to realize the bit-based encryption, the values are obtained from the voice file consisting of float values with appropriate sampling step and converted into binary form. With random bit sequences past all NIST 800-22 randomness tests obtained from the RNG, the voice file in the binary form is encrypted. XOR operation is used in encryption process. After the encryption operation, the encrypted binary bit array is changed to the float form to generate the encrypted voice file. After the encrypted voice data is sent to the receiver side in this way, the decryption process is performed by applying the reverse operations in the encryption. Thus, the original voice file is attained on the receiving side.
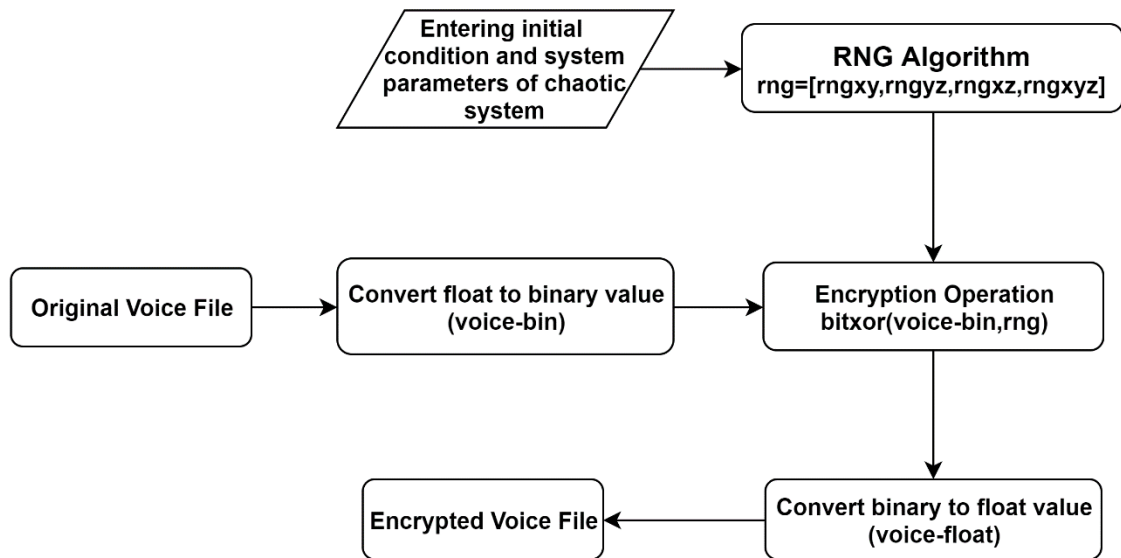
Figure 12. The block diagram of encryption process.

The voice files in encryption procedure are shown in Figure 13. The original, encrypted and decrypted voice file is demonstrated in Figure 13a–c, respectively. When comparing the original and encrypted voice file in Figure 13a,b; it is seen that a very different file is gotten than the original and the encryption process is successful. When Figure 13a,c are examined, it is observed that the decryption procedure is successful. Figure 14 shows the frequency spectrum analysis results of the encryption process. Frequency spectrum analysis is carried out to determine the frequency range of voice files. To determine the success of the encryption process, frequency spectrum analyzes are performed on original and encrypted voice files. The spectrum analysis results of original and encrypted voice files are illustrated in Figure 14a,b. If we compare these two graphs, it seems that the encrypted voice file has a rather wide frequency spectrum range than the original. When these results are evaluated, it shows the success of the encryption process.
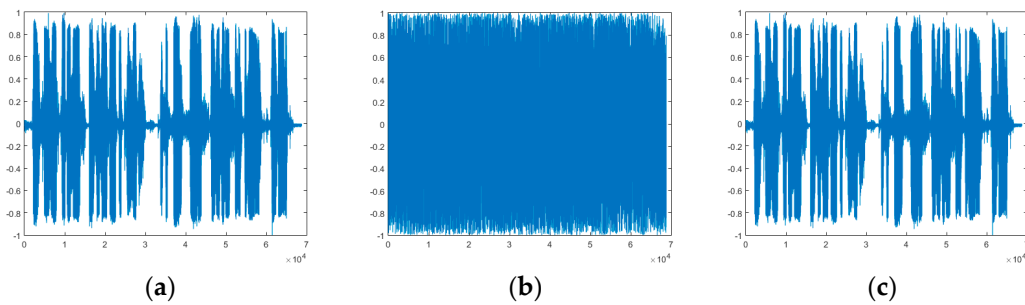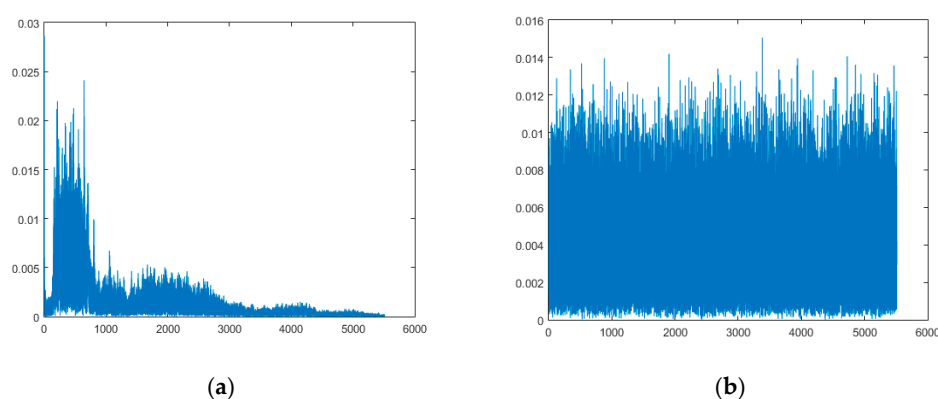

Figure 13. The voice file (**a**) original; (**b**) encrypted; (**c**) decrypted.

Figure 14. The spectrum analysis outcomes of original and encrypted voice files. (**a**) Original, (**b**) Encrypted.

5. Conclusions and Discussion

In this article, a new chaotic system with hyperbolic sinusoidal nonlinearity is designed. The proposed system belongs to a new category of dynamical systems with hidden chaotic flows, which assist in further understanding of chaotic attractors and also to use them in interesting applications like cryptography and secure communication schemes. The feature of hidden chaotic attractors, such as in systems with line of equilibria or in systems with no equilibrium point, makes them more suitable for the aforementioned applications, due to the fact that using systems with hidden attractors adds complexity to the dynamical system, which is used in this kind of applications. Therefore, in this work a voice encryption scheme, which is based on the specific systems was studied. Based on the variations of parameters of the system, this flow presented two classes of hidden attractors (with line of equilibria and no equilibrium point) plus a self-excited attractor, which has been reported to the literature for the first time. Dynamical behavior of the proposed system was explored and its bifurcation diagram and spectrum of Lyapunov exponents were propounded. For the appropriate selection of the parameters, the flow could display periodic oscillations and double-scroll chaos attractors. The system's electronic simulation investigated the confirmation of the double-scroll chaos attractor in real word. Via the proposed chaotic system, a novel RNG design was realized and random number generation was performed. NIST 800-22 randomness examinations were employed to the produced numbers and it was determined that all tests passed. By using RNG design, a novel voice encryption algorithm was established and encryption process was done. Frequency spectrum analysis of the voice encryption procedure was executed. In line with the analysis outcomes, it has been found that the new RNG design produces high random numbers and that the suggested encryption algorithm effectively achieves the encryption process. Therefore, authors aim with this work to attract the interest of the research community in the use of chaotic dynamical systems with hidden attractors in encryption schemes, as the results are proved to be very promising. Finally, as a future plan, the hardware implementation of the specific approach has been planned.

Author Contributions: S.M. was responsible for formal analysis and writing—original draft preparation. C.K.V. and Ü.Ç. were responsible to conceptualization, methodology, and software. S.K. was responsible for software, supervision and editing. All authors have read and agreed to the published version of the manuscript.

Appendix A

Algorithm 1 RNG Design Algorithm Pseudo Code

1:   **Start**
2:   rngx=[[] rngy=[[] rngz=[[] rngxy=[[] rngyz=[[] rngxz=[[] rngxyz=[[]
3:   Entering system parameters and initial conditions of chaotic systems
4:   Determination of the appropriate value of (Δh=0.001)
5:   **while** i<=1000000 **do**
6:   Sampling with determination Δh value
7:   Solving the chaotic system using RK4 algorithm
8:   Obtaining time series float values (x,y,z) (each value 15 digit)
9:   **for** k = 0 **to** 14 **do**
10:      rngx[i]=mod(x[k], 2);
11:      rngy[i]=mod(y[k], 2);
12:      rngz[i]=mod(z[k], 2);
13:         i=i+1
14:     **end for**
15:   **end while**
16:   rngxy=bitxor(rngx, rngy);
17:   rngyz=bitxor(rngy, rngz);
18:   rngxz=bitxor(rngx, rngz);
19:   rngxyz = bitxor(rngxy, rngz);
20:   The implementation of NIST tests for each new array (rngxy, rngyz, rngxz, rngxyz)
21:   rng=[rngxy,rngyz,rngxz,rngxyz]
22:   **End**

References

1. Hua, Z.; Zhou, B.; Zhou, Y. Sine-Transform-Based Chaotic System With FPGA Implementation. *IEEE Trans. Ind. Electron.* **2018**, *65*, 2557–2566. [CrossRef]
2. Thoai, V.P.; Kahkeshi, M.S.; Huynh, V.V.; Ouannas, A.; Pham, V.-T. A Nonlinear Five-Term System: Symmetry, Chaos, and Prediction. *Symmetry* **2020**, *12*, 865. [CrossRef]
3. Chain, K.; Kuo, W.-C. A new digital signature scheme based on chaotic maps. *Nonlinear Dyn.* **2013**, *74*, 1003–1012. [CrossRef]
4. Muthukumar, P.; Balasubramaniam, P.; Ratnavelu, K. Sliding mode control design for synchronization of fractional order chaotic systems and its application to a new cryptosystem. *Int. J. Dyn. Control* **2017**, *5*, 115–123. [CrossRef]
5. Deng, Y.; Hu, H.; Liu, L. Feedback control of digital chaotic systems with application to pseudorandom number generator. *Int. J. Mod. Phys. C* **2015**, *26*, 1550022. [CrossRef]
6. Castro-Ramírez, J.; Martínez-Guerra, R.; Cruz-Victoria, J.C. A new reduced-order observer for the synchronization of nonlinear chaotic systems: An application to secure communications. *Chaos Interdiscip. J. Nonlinear Sci.* **2015**, *25*, 103128. [CrossRef]
7. Wang, G.; Chen, D.; Lin, J.; Chen, X. The application of chaotic oscillators to weak signal detection. *IEEE Trans. Ind. Electron.* **1999**, *46*, 440–444. [CrossRef]
8. Sakthivel, R.; Santra, S.; Anthoni, S.M.; Kuppili, V. Synchronisation and anti-synchronisation of chaotic systems with application to DC–DC boost converter. *IET Gener. Transm. Distrib.* **2017**, *11*, 959–967. [CrossRef]
9. Chen, E.; Min, L.; Chen, G. Discrete Chaotic Systems with One-Line Equilibria and Their Application to Image Encryption. *Int. J. Bifurc. Chaos* **2017**, *27*, 1750046. [CrossRef]

10. Glushkov, A.V.; Khetselius, O.; Brusentseva, S.V.; Zaichko, P.A.; Ternovsky, V.B. Studying interaction dynamics of chaotic systems within a non-linear prediction method: Application to neurophysiology. *Adv. Neural Netw. Fuzzy Syst. Artif. Intell.* **2014**, *21*, 69–75.

11. Aguilar-López, R.; Martínez-Guerra, R.; Perez-Pinacho, C.A. Nonlinear observer for synchronization of chaotic systems with application to secure data transmission. *Eur. Phys. J. Spec. Top.* **2014**, *223*, 1541–1548. [CrossRef]

12. Radwan, A.; Moaddy, K.; Salama, K.N.; Momani, S.; Hashim, I. Control and switching synchronization of fractional order chaotic systems using active control technique. *J. Adv. Res.* **2014**, *5*, 125–132. [CrossRef] [PubMed]

13. Boulkroune, A.; Bouzeriba, A.; Hamel, S.; Bouden, T. Adaptive fuzzy control-based projective synchronization of uncertain nonaffine chaotic systems. *Complexity* **2015**, *21*, 180–192. [CrossRef]

14. Mobayen, S. Finite-time stabilization of a class of chaotic systems with matched and unmatched uncertainties: An LMI approach. *Complexity* **2016**, *21*, 14–19. [CrossRef]

15. Ma, D.; Sun, Q.; Li, X. Synchronization of master-slave chaotic system with coupling time-varying delay based on sampled-data control. In Proceedings of the Control and Decision Conference (CCDC), 2015 27th Chinese, Qingdao, China, 23–25 May 2015; pp. 6545–6550.

16. Xiong, W.; Huang, J. Finite-time control and synchronization for memristor-based chaotic system via impulsive adaptive strategy. *Adv. Differ. Equ.* **2016**, *2016*, 101. [CrossRef]

17. Song, Q.; Huang, T. Stabilization and synchronization of chaotic systems with mixed time-varying delays via intermittent control with non-fixed both control period and control width. *Neurocomputing* **2015**, *154*, 61–69. [CrossRef]

18. Mobayen, S.; Baleanu, D.; Tchier, F. Second-order fast terminal sliding mode control design based on LMI for a class of non-linear uncertain systems and its application to chaotic systems. *J. Vib. Control* **2017**, *23*, 2912–2925. [CrossRef]

19. Wei, Z. Dynamical behaviors of a chaotic system with no equilibria. *Phys. Lett. A* **2011**, *376*, 102–108. [CrossRef]

20. Jafari, S.; Sprott, J.C.; Golpayegani, S. Elementary quadratic chaotic flows with no equilibria. *Phys. Lett. A* **2013**, *377*, 699–702. [CrossRef]

21. Wang, X.; Chen, G. A chaotic system with only one stable equilibrium. *Commun. Nonlinear Sci. Numer. Simul.* **2012**, *17*, 1264–1272. [CrossRef]

22. Molaie, M.; Jafari, S.; Sprott, J.C.; Golpayegani, S. Coexisting hidden attractors in a 4-D simplified Lorenz system. *Int. J. Bifurc. Chaos* **2013**, *23*, 1350188. [CrossRef]

23. Shilnikov, L.P. A case of the existence of a denumerable set of periodic motions. *Sov. Math.* **1965**, *24*, 163–166.

24. Leonov, G.A.; Kuznetsov, N.V.; Kuznetsova, O.A.; Seledzhi, S.M.; Vagaitsev, V.I. Hidden oscillations in dynamical systems. *Trans. Syst. Contr.* **2011**, *6*, 54–67.

25. Leonov, G.A.; Kuznetsov, N.V.; Vagaitsev, V.I. Hidden attractor in smooth chua systems. *Phys. D Nonlinear Phenom.* **2012**, *241*, 1482–1486. [CrossRef]

26. Leonov, G.A.; Kuznetsov, N.V. Hidden attractors in dynamical systems. From hidden oscillations in Hilbert Kolmogorov, Aizerman, and Kalman problems to hidden chaotic attractor in Chua circuits. *Int. J. Bifurc. Chaos* **2013**, *23*, 1330002. [CrossRef]

27. Wang, Z.; Volos, C.; Kingni, S.T.; Azar, A.T.; Pham, V.-T. Four-wing attractors in a novel chaotic system with hyperbolic sine nonlinearity. *Opt. Int. J. Light Electron Opt.* **2017**, *131*, 1071–1078. [CrossRef]

28. Pham, V.-T.; Volos, C.; Kingni, S.T.; Kapitaniak, T.; Jafari, S. Bistable Hidden Attractors in a Novel Chaotic System with Hyperbolic Sine Equilibrium. *Circuitssyst. Signal Process.* **2017**, *37*, 1028–1043. [CrossRef]

29. Kuznetsov, A.; Kuznetsov, S.; Mosekilde, E.; Stankevich, N. Co-existing hidden attractors in a radio-physical oscillator system. *J. Phys. A Math.* **2015**, *48*, 125101. [CrossRef]

30. Zhusubaliyev, Z.T.; Mosekilde, E. Multistability and hidden attractors in a multilevel DC/DC converter. *Math. Comput. Simul.* **2015**, *109*, 32–45. [CrossRef]

31. Kiseleva, M.A.; Kuznetsov, N.V.; Leonov, G.A. Hidden attractors in electromechanical systems with and without equilibria. *IFAC Pap.* **2016**, *49*, 51–55. [CrossRef]

32. Zhusubaliyev, Z.T.; Mosekilde, E.; Rubanov, V.G.; Nabokov, R.A. Multistability and hidden attractors in a relay system with hysteresis. *Phys. D Nonlinear Phenom.* **2015**, *306*, 6–15. [CrossRef]

33. Yu, M.; Sun, K.; Liu, W.; He, S. A hyperchaotic map with grid sinusoidal cavity. *Chaossolitons Fractals* **2018**, *106*, 107–117. [CrossRef]

34. Zhang, X.; Li, C.; Lei, T.; Liu, Z.; Tao, C. A symmetric controllable hyperchaotic hidden attractor. *Symmetry* **2020**, *12*, 550. [CrossRef]

35. Sadkhan, S.B.; Ali, H. A proposed speech scrambling based on hybrid chaotic key generators. In Proceedings of the 2016 Al-Sadeq IEEE International Conference on Multidisciplinary in IT and Communication Science and Applications (AIC-MITCSA), Al-Najaf, Iraq, 9–10 May 2016; pp. 1–6.

36. Mobayen, S.; Vaidyanathan, S.; Sambas, A.; Kacar, S.; Çavuşoğlu, Ü. A novel chaotic system with boomerang-shaped equilibrium, its circuit implementation and application to sound encryption. *Iran. J. Sci. Technol. Trans. Electr. Eng.* **2019**, *43*, 1–12.

37. Raheema, A.M.; Sadkhan, S.B.; Sattar, S.M.A. Design and implementation of speech encryption based on hybrid chaotic maps. In Proceedings of the 2018 IEEE International Conference on Engineering Technology and Their Applications (IICETA), Al-Najaf, Iraq, 8–9 May 2018; pp. 112–117.

38. Nosrati, K.; Volos, C. Bifurcation Analysis and Chaotic Behaviors of Fractional-Order Singular Biological Systems. In *Nonlinear Dynamical Systems with Self-Excited and Hidden Attractors*; Springer: Berlin/Heidelberg, Germany, 2018; pp. 3–44.

39. Wu, F.; Ma, J. The chaos dynamic of multiproduct Cournot duopoly game with managerial delegation. *Discret. Dyn. Nat. Soc.* **2014**, *2014*. [CrossRef]

40. Barrera, J.; Flores, J.J.; Fuerte-Esquivel, C. Generating complete bifurcation diagrams using a dynamic environment particle swarm optimization algorithm. *J. Artif. Evol. Appl.* **2007**, *2008*. [CrossRef]

41. Ouannas, A.; Khennaoui, A.A.; Wang, X.; Pham, V.-T.; Boulaaras, S.; Momani, S. Bifurcation and chaos in the fractional form of Hénon-Lozi type map. *Eur. Phys. J. Spec. Top.* **2020**, *229*, 2261–2273. [CrossRef]

42. Zhu, X.; Du, W.-S. New chaotic systems with two closed curve equilibrium passing the same point: Chaotic behavior, bifurcations, and synchronization. *Symmetry* **2019**, *11*, 951. [CrossRef]

43. Awrejcewicz, J.; Krysko, A.V.; Erofeev, N.P.; Dobriyan, V.; Barulina, M.A.; Krysko, V.A. Quantifying chaos by various computational methods. Part 1: Simple systems. *Entropy* **2018**, *20*, 175. [CrossRef]

44. Kong, G.; Zhang, Y.; Khalaf, A.J.M.; Panahi, S.; Hussain, I. Parameter estimation in a new chaotic memristive system using ions motion optimization. *Eur. Phys. J. Spec. Top.* **2019**, *228*, 2133–2145. [CrossRef]

45. Huang, W.; Kamenski, L.; Lang, J. Conditioning of implicit Runge–Kutta integration for finite element approximation of linear diffusion equations on anisotropic meshes. *J. Comput. Appl. Math.* **2019**. [CrossRef]

46. Wolf, A.; Swift, J.B.; Swinney, H.L.; Vastano, J.A. Determining Lyapunov exponents from a time series. *Phys. D Nonlinear Phenom.* **1985**, *16*, 285–317. [CrossRef]

47. Bouali, S.; Buscarino, A.; Fortuna, L.; Frasca, M.; Gambuzza, L. Emulating complex business cycles by using an electronic analogue. *Nonlinear Anal. Real World Appl.* **2012**, *13*, 2459–2465. [CrossRef]

48. Banerjee, T.; Biswas, D. Theory and experiment of a first-order chaotic delay dynamical system. *Int. J. Bifurc. Chaos* **2013**, *23*, 1330020. [CrossRef]

49. Zhou, W.-J.; Wang, Z.-P.; Wu, M.-W.; Zheng, W.-H.; Weng, J.-F. Dynamics analysis and circuit implementation of a new three-dimensional chaotic system. *Opt. Int. J. Light Electron Opt.* **2015**, *126*, 765–768. [CrossRef]

50. Lai, Q.; Wang, L. Chaos, bifurcation, coexisting attractors and circuit design of a three-dimensional continuous autonomous system. *Opt. Int. J. Light Electron Opt.* **2016**, *127*, 5400–5406. [CrossRef]

51. Gokyildirim, A.; Uyaroglu, Y.; Pehlivan, I. A novel chaotic attractor and its weak signal detection application. *Opt. Int. J. Light Electron Opt.* **2016**, *127*, 7889–7895. [CrossRef]

52. Hajipour, A.; Tavakoli, H. Analysis and circuit simulation of a novel nonlinear fractional incommensurate order financial system. *Opt. Int. J. Light Electron Opt.* **2016**, *127*, 10643–10652. [CrossRef]

53. Wang, Y.; Wong, K.-W.; Liao, X.; Chen, G. A new chaos-based fast image encryption algorithm. *Appl. Soft Comput.* **2011**, *11*, 514–522. [CrossRef]

54. Çavuşoğlu, Ü.; Kaçar, S.; Pehlivan, I.; Zengin, A. Secure image encryption algorithm design using a novel chaos based S-Box. *Chaossolitons Fractals* **2017**, *95*, 92–101. [CrossRef]

55. Bakhache, B.; Ghazal, J.M.; El Assad, S. Improvement of the security of zigbee by a new chaotic algorithm. *IEEE Syst. J.* **2014**, *8*, 1024–1033. [CrossRef]

56. Khan, M. A novel image encryption scheme based on multiple chaotic S-boxes. *Nonlinear Dyn.* **2015**, *82*, 527–533. [CrossRef]

57. Çavuşoğlu, Ü.; Zengin, A.; Pehlivan, I.; Kaçar, S. A novel approach for strong S-Box generation algorithm design based on chaotic scaled Zhongtang system. *Nonlinear Dyn.* **2017**, *87*, 1081–1094. [CrossRef]

58. Hua, Z.; Zhou, Y.; Pun, C.-M.; Chen, C.P. 2D Sine Logistic modulation map for image encryption. *Inf. Sci.* **2015**, *297*, 80–94. [CrossRef]

59. Rukhin, A.; Soto, J.; Nechvatal, J.; Smid, M.; Barker, E. *A Statistical Test Suite for Random and Pseudorandom Number Generators for Cryptographic Applications*; Booz-Allen and Hamilton Inc Mclean Va: McLean, VA, USA, 2001.

Publisher's Note: MDPI stays neutral with regard to jurisdictional claims in published maps and institutional affiliations.